

Variability of Atlantic Meridional Overturning Circulation in FGOALS-g2

HUANG Wenyu¹, WANG Bin^{*1,2}, LI Lijuan², DONG Li², LIN Pengfei², YU Yongqiang²,
ZHOU Tianjun², LIU Li¹, XU Shiming¹, XIA Kun¹, PU Ye², WANG Lu², LIU Mimi²,
SHEN Si², HU Ning², WANG Yong², SUN Wenqi², and DONG Fang¹

¹Ministry of Education Key Laboratory for Earth System Modeling, Center for Earth System Science,
Tsinghua University, Beijing 100084

²State Key Laboratory of Numerical Modeling for Atmospheric Sciences and Geophysical Fluid Dynamics,
Institute of Atmospheric Physics, Chinese Academy of Sciences, Beijing 100029

(Received 15 July 2012; revised 4 March 2013; accepted 25 March 2013)

ABSTRACT

The variability of Atlantic Meridional Overturning Circulation (AMOC) in the pre-industrial control experiment of the Flexible Global Ocean–Atmosphere–Land System model, Grid-point Version 2 (FGOALS-g2) was investigated using the model outputs with the most stable state in a 512-yr time window from the total 1500-yr period of the experiment. The period of AMOC in FGOALS-g2 is double peaked at 20 and 32 years according to the power spectrum, and 22 years according to an auto-correlation analysis, which shows very obvious decadal variability. Like many other coupled climate models, the decadal variability of AMOC in FGOALS-g2 is closely related to the convection that occurs in the Labrador Sea region. Deep convection in the Labrador Sea in FGOALS-g2 leads the AMOC maximum by 3–4 years. The contributions of thermal and haline effects to the variability of the convection in three different regions [the Labrador, Irminger and Greenland–Iceland–Norwegian (GIN) Seas] were analyzed for FGOALS-g2. The variability of convection in the Labrador and Irminger Seas is thermally dominant, while that in the colder GIN Seas can be mainly attributed to salinity changes due to the lower thermal expansion. By comparing the simulation results from FGOALS-g2 and 11 other models, it was found that AMOC variability can be attributed to salinity changes for longer periods (longer than 35 years) and to temperature changes for shorter periods.

Key words: AMOC, decadal variability, deep convection, FGOALS-g2

Citation: Huang, W. Y., and Coauthors, 2014: Variability of Atlantic meridional overturning circulation in FGOALS-g2. *Adv. Atmos. Sci.*, **31**(1), 95–109, doi: 10.1007/s00376-013-2155-7.

1. Introduction

Atlantic Meridional Overturning Circulation (AMOC) is one of the most important large-scale ocean current systems for the global climate (Hofmann and Rahmstorf, 2009) and can be characterized as follows: (1) in the upper Atlantic Ocean, warm and saline water moves northward from the Equator towards northern high latitudes, and a part of these northward moving surface waters is derived from the Southern Ocean due to Ekman transport driven by strong westerly winds (Delworth et al., 2008); (2) in the deepest part of the Atlantic Ocean, there is a cold water mass (Antarctic Bottom Water), which is derived from the cold dense water descending along the continental margin of Antarctica in austral winter (Gordon, 2009); (3) in the North Atlantic Ocean, the northward moving surface water descends into the deep ocean and forms North Atlantic Deep Water (NADW) due to heat loss and brine-release from sea ice formation in boreal

winter (Van Aken, 2007); and (4) NADW is carried southward, upwells to the upper ocean in the low latitudes due to thermocline cross-isopycnal mixing, and in the Southern Ocean due to wind-driven mixing, and thus closes the water cycle (Kuhlbrodt et al., 2007). AMOC transports about a quarter of total global ocean–atmosphere northward heat flux in the Northern Hemisphere (Bryden and Imawaki, 2001). Owing to its important role in modulating the energy balance, as well as there being serious consequences should it break down (Delworth et al., 2008), AMOC draws much attention from the research community.

AMOC is directly or indirectly related to many climate systems or phenomena, such as Atlantic Multi-decadal Oscillation (AMO) (Latif et al., 2004), variability of Arctic sea ice (Mahajan et al., 2011), and El Niño–Southern Oscillation (Timmermann et al., 2005, 2007). Among these relationships, the link between AMOC and AMO is subject to debate because of a shortage of long-term observation data of AMOC. On the one hand, the decadal variability of AMO is attributed to the internal variability of the climate system and claimed to be closely related to the variability of AMOC

* Corresponding author: WANG Bin
E-mail: wab@mail.tsinghua.edu.cn

(Delworth and Mann, 2000; Knight et al., 2005; Zhang, 2007); while on the other hand, the important role of external forcing, such as volcanoes, on the variability of AMO has been emphasized (e.g., Otterå et al., 2010). At least, AMOC is likely to be one of the origins of the decadal variability in the North Atlantic Ocean (Latif and Keenlyside, 2011).

Because of the long-term “memory” and the very important role of AMOC in poleward heat transport, AMOC is a potential indicator of future climate change (Huang et al., 2012). Although the relationship between AMOC and AMO is not very clear, an understanding of the decadal variability of AMOC will at least benefit our knowledge of internal climate variability to a certain extent.

Studying the variability of AMOC using observational data is the first choice. However, because the ocean is opaque to electromagnetic radiation (Wunsch and Stammer, 1998) and AMOC has a wide geographical distribution, it is very difficult to accurately describe its 2D or 3D structure. Observations of AMOC are always made at specific latitudes, defined by the particular field experiment involved, such as the RAPID-MOCHA program (Cunningham et al., 2007; Kanzow et al., 2009, 2010; Johns et al., 2011), as well as *in situ* floats and satellite altimeters (Willis, 2010). In addition, the length of the dataset derived from such experiments is too short to study the decadal variability of AMOC (e.g., the RAPID-MOCHA program provided data from April 2004 to April 2008).

Coupled climate models are indispensable tools for studying the decadal variability of AMOC and other climate phenomena, especially in cases where sufficient observations are unavailable (Delworth et al., 1993; Dong and Sutton, 2005). Because of the different resolutions and physical parameterizations adopted by different climate models, the range of peak periods of AMOC reported is wide (Danabasoglu, 2008). In ocean models, the most relevant parameterization schemes to periods of AMOC are the vertical mixing scheme and overflow scheme (Danabasoglu et al., 2012), for the following two reasons. (1) Vertical mixing unstratifies the water column and favors deep convection (Kuhlbrodt et al., 2007), which is a central cause of deep water formation (Bentsen et al., 2004; Jungclaus et al., 2005; Danabasoglu, 2008; Danabasoglu et al., 2012), i.e., NADW (an important part of AMOC). (2) Overflow across the Greenland-Scotland Ridge transfers deep water formed in the GIN (Greenland-Iceland-Norwegian) Seas southward into the Labrador Sea (Hansen et al., 2001; Medhaug et al., 2012). It should be noted that the heat losses from ocean to atmosphere, which are triggered by the frequent winter storms in the North Atlantic Ocean, are essential to the occurrence of deep convection (Marshall and Schott, 1999).

To study the internal variability of AMOC, experiments under non-evolving forcing (e.g., greenhouse gas concentrations fixed at the pre-industrial level) with long-term integration (usually more than 1000 years) must be carried out. However, not all simulated data can be used for such analysis because of the special features in different phases of the process, such as the “spin up” (at the initial time of integra-

tion) and “climate drift” (after long-term integration) phases. Until recently, studies of AMOC variability have not provided a method to determine these phases. In analyses of AMOC based on present-day control runs of the Community Climate System Model, version 3 (CCSM3) (700 years), two periods have been used in different studies (Danabasoglu, 2008; Kwon and Frankignoul, 2012). However, no quantitative method to identify the boundaries of these time periods has been applied. Another example comes from an analysis of AMOC variability using version 3 of the Hadley Center Coupled Model (HadCM3), in which the entire simulation was used (Dong and Sutton, 2005). Therefore, how best to choose the time window for AMOC analysis remains an open question, and this is the topic we set out to address in the present reported work.

The main goal of the paper is to analyze the internal variability of AMOC with a focus on the decadal signal and associated mechanism in the Flexible Global Ocean-Atmosphere-Land System model, Grid-point Version 2 (FGOALS-g2), and the remainder of the text is organized as follows. In section 2, FGOALS-g2 and the data selection from the model simulation are described. The decadal variability of AMOC and the associated mechanism are detailed in section 3, wherein the role of deep convection is emphasized and the effects of salinity and temperature on the deep convection are analyzed. Similar analyses have been performed for other climate models. Therefore, in section 4, we compare and discuss the characteristics of AMOC in different climate models based on the present literature. The final section (section 5) provides a summary and sets out the main conclusions of the work.

2. Model description and data selection

2.1. Model description

FGOALS-g2 is a coupled climate model developed by the LASG/CESS team (State Key Laboratory of Atmospheric Sciences and Geophysical Fluid Dynamics/Center for Earth System Science). The four components of FGOALS-g2 (Li et al., 2013a), i.e., the atmospheric, land-surface, ocean, and sea-ice components, are coupled together through Coupler 6 (CPL6) from the National Center for Atmospheric Research (NCAR) (Craig et al., 2005). The atmospheric component is the Grid-point Atmospheric Model of the IAP (Institute of Atmospheric Physics)/LASG, version 2.0 (GAMIL2.0) and has 26 layers in the vertical direction (Wang et al., 2004; Li et al., 2013b), while the land-surface component is the Community Land Model, version 3 (CLM3.0) and has 10 soil layers in the vertical direction (Oleson et al., 2004). Both have the same horizontal resolution ($2.8^\circ \times 2.8^\circ$). The ocean component is the LASG/IAP Climate Ocean Model, version 2 (LICOM2.0). It has a nominal horizontal resolution of 1° with a meridional refinement in the equatorial region, approaching a minimum 0.5° grid spacing, and 30 layers in the vertical direction with a resolution of 10 m in the upper 150 m (Liu et al., 2012). The vertical mixing scheme in LICOM2.0

is the second-order closure model of Canuto et al. (2001, 2002), and no overflow parameterization scheme is included. The sea-ice component is CICE4-LASG, an improved version of CICE4 (Community Ice Code Version 4), and has the same horizontal resolution as the ocean component (Liu, 2010). It has been documented that low AMOC, with a maximum of about 10 Sv ($1 \text{ Sv} = 10^6 \text{ m}^3\text{s}^{-1}$) exists in version 1 of FGOALS (FGOALS-g1) (Medhaug and Furevik, 2011). An improved representation of AMOC in FGOALS-g2 compared to FGOALS-g1 will be illustrated in this paper.

2.2. AMOC index

Traditionally, AMOC is defined as the zonally-integrated annual-mean overturning stream function in depth space. However, it has been suggested that defining AMOC in potential density space may be better in terms of representing the transportation of water masses (Döös and Webb, 1994; Treguier et al., 2007; Dufour et al., 2012), and measuring the changes of AMOC in subpolar regions where the northward and southward flows with different densities take place at similar depths (Zhang, 2010a, b). However, because we intend to directly compare the results of FGOALS-g2 with those of other models in the literature, and given that the studies in which those model results have been presented largely defined AMOC according to depth space, we have chosen to do the same in the present work.

The AMOC index used throughout this paper, unless otherwise stated, is defined as the maximum of meridional overturning stream function between 15° and 65°N and below 500 m in depth, which serves to exclude surface-wind-driven overturning (Schott et al., 2004; Medhaug and Furevik, 2011).

2.3. Method for determining the most stable state

A question that always arises in a control simulation is: when does the coupled model enter its balanced state? Factors such as sea surface temperature, sea surface salinity, sea ice area and sea ice volume are often used as indicators of when the simulation reaches a balanced state (Gordon et al., 2000; Delworth et al., 2006; Doney et al., 2006; Phipps et al., 2011). In fact, the equilibrium of AMOC is not only a good representation of the energy balance between the low and high latitudes, but also an indicator of when air-sea interaction and the deep ocean reach a relatively stable state. Therefore, the AMOC index is used here to identify the most stable state. Typically, when analyzing the internal decadal variability of AMOC, the long-term trends of the AMOC index and other physical quantities are removed (detrending) before detailed analysis such as correlation, regression and spectral analysis can be done. However, when the linear trend is large, uncertainty arises in the detrending process, i.e., the decadal signal is easily contaminated. Thus, a period of stable AMOC signal needs to be identified.

There are about 1500 model years in the pre-industrial control experiment of FGOALS-g2. However, not all parts of the simulation are useful, such as the “spin-up” process at the initial time and the long-term “climate drift” (Sen Gupta et

al., 2012). In this paper, to determine within which time window the climate state is most stable, a new method named the “running standard deviation method” is proposed, which is based on the standard deviation (SD) of a running time window of the AMOC index. The only adjustable parameter is the length of the time window, which can be set by the user. The details of the new method are as follows: (1) assume that the length of total available data is N (units: years), and the length of the adjustable time window is M (units: years), wherein M must be an even number; (2) let AMOC-SD (x) be the SD of the AMOC index for each continuous M -year subperiod ($[x - M/2 + 1], [x + M/2]$) in the N -year period, and x the center year of the subperiod, which is to be determined; and (3) the M -year time window ($[x - M/2 + 1], [x + M/2]$) is obtained as the balanced state, when AMOC-SD (x) reaches its minimum at some point, x .

The goals of this new method are to remove the initial “spin-up” and the final “climate drift” periods. SD measures the variance of a time series and thus can be taken as a measurement of the stability. We use an analysis window with a length of 512 (the power of 2, suitable for spectral and wavelet analyses) years running along the 1500-yr time series of the AMOC index (see Fig. 1a). Sensitivities of SD and the trend of AMOC index values due to changes in the length of the time window have been analyzed (not shown).

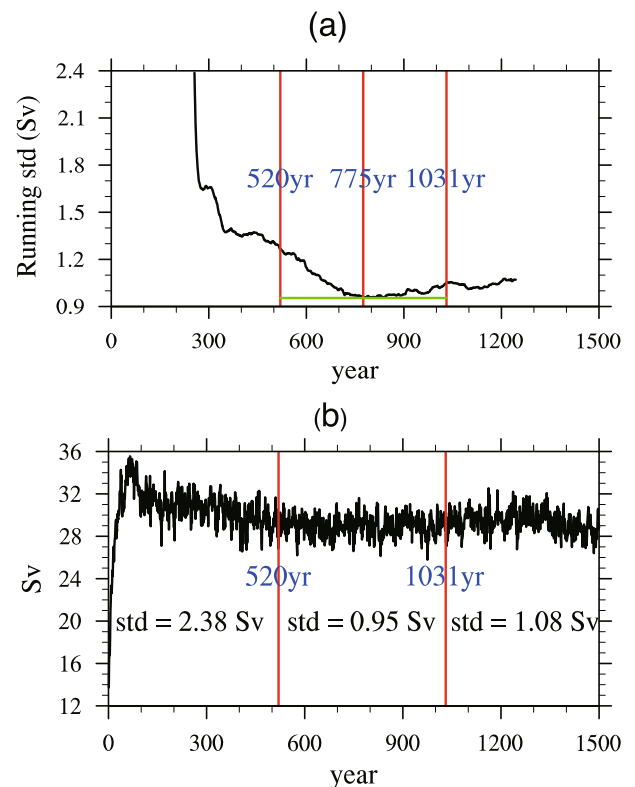


Fig. 1. (a) Diagram showing the running SD method. The period from year 520 to 1031 has the minimum SD of 0.95 Sv (see section 2.3 of the text for further details). (b) Time series of the AMOC index (units: Sv), which is defined as the maximum of meridional stream function in the Atlantic Ocean from 15°N to 65°N and below 500 m.

In the sensitivity study, the length of the time window varied from 100 to 1200 years, with a time interval of 100 years. As the length of the time window increased, the SD increased almost uniformly. The minimum trend of the AMOC index was obtained as $7.1 \times 10^{-5} \text{ Sv yr}^{-1}$ when the length was 500 years, which supports the choice of 512 years to be used in this paper. The minimum SD (see Fig. 1b) was found in the 512-year window with year 775 as the center, i.e., the window started at year 520 and ended at year 1031. The minimum SD and linear trend gradient (LTG) in this period were 0.95 Sv and $8.5 \times 10^{-6} \text{ Sv yr}^{-1}$, respectively. In contrast, the “spin-up” period (from year 1 to 519) was marked by an SD of 2.38 Sv and an LTG of $-2.1 \times 10^{-3} \text{ Sv yr}^{-1}$, while the “climate drift” period (from year 1032 to 1500) with an SD of 1.08 Sv and an LTG of $-1.8 \times 10^{-3} \text{ Sv yr}^{-1}$. The period from year 520 to 1031 will be used for investigating the variability of AMOC.

3. Decadal variability of AMOC and its associated mechanism

3.1. Mean State of AMOC

Observations of AMOC at 26.5°N from the RAPID-MOCHA program (Cunningham et al., 2007; Johns et al., 2011) and at 41°N estimated using data from in situ floats and satellite altimeters (Willis, 2010) are used to evaluate the performance of FGOALS-g2. The annually averaged value at 26.5°N given by Cunningham et al. (2007) is 18.7 Sv with an SD of 5.6 Sv, while that estimated by Johns et al. (2011) at the same latitude using the same data is 18.5 Sv. The annually averaged AMOC value at 41°N from 2004 through 2006 is about 15.5 Sv with an SD of 2.4 Sv (Willis, 2010). The 2D structure of AMOC in FGOALS-g2 is shown in Fig. 2a. Compared with observations, FGOALS-g2 overestimates the maximum values of AMOC at both 26.5°N and 41°N (us-

ing the 512-yr monthly average), and the simulated values are 22.9 Sv and 24.7 Sv, which are about 4.2 Sv and 9.2 Sv larger, respectively. Despite the existence of this bias, the current version outperforms the previous version, FGOALS-g1, which produces much weaker AMOC with a maximum less than 10 Sv at 26.5°N . The improved representation of AMOC can be attributed to the adoption of the Canuto vertical mixing scheme (Canuto et al., 2001, 2002) in LICOM2.0, which includes the effects of shear-driven mixing, double diffusion and internal wave breaking (Liu et al., 2012). In contrast, the Richardson number dependent scheme (Pacanowski and Philander, 1981) (the PP scheme) in the previous version of LICOM2.0 only includes the effects of shear-driven mixing.

The northward heat transport corresponding to AMOC in FGOALS-g2 is illustrated in Fig. 2b. The northward ocean heat transport estimated by Trenberth et al. (2001) using various reanalyzed surface heat fluxes are taken here for comparison. The northward heat transport in the low latitudes of the Atlantic Ocean (30°S – 30°N) is simulated well in FGOALS-g2. However, it is overestimated in the high latitudes, which is closely related to the overestimation of AMOC.

The average depth of AMOC maxima in different models (coupled or single ocean models) from the literature is taken here for comparison (see Table 1). The averaged depth of the AMOC maximum of the 12 models in Table 1 is 1044 m. In comparison, the observed depth at 26.5°N is 1050 m in the RAPID-MOCHA program, which was estimated using the data provided by Johns et al. (2011). However, the simulated depth by FGOALS-g2 is 731 m, which is shallower than the average. This bias may partially result from the setting of the vertical levels in the ocean model of FGOALS-g2 near 731 m, which are 354 m, 510 m, 731 m, 1021 m, 1385 m and 1821 m (the depths of the interfaces of the model layers). Increasing the vertical resolution near to 1000 m may be helpful to reduce the bias. The latitude of maximum AMOC varies from model to model, and that of FGOALS-g2 is 36.5°N , close to

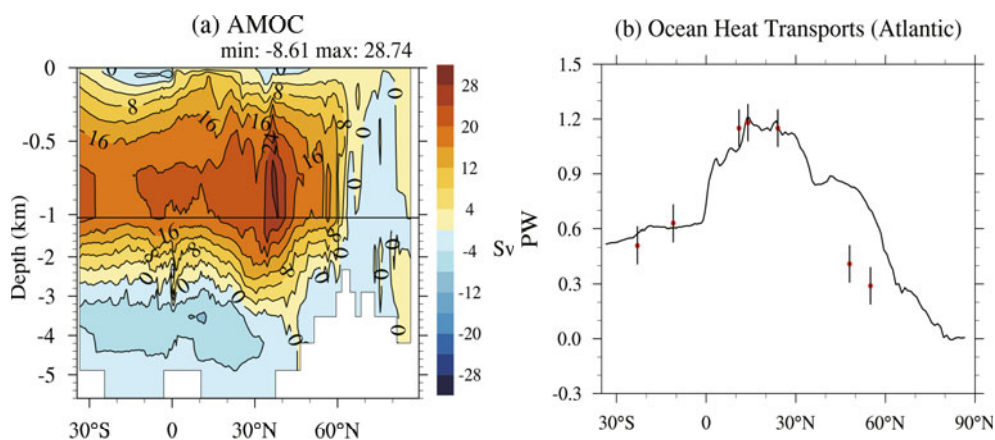


Fig. 2. (a) 2D AMOC averaged from year 520 to 1031 on the latitude–depth plane (units: Sv), where a positive (negative) value indicates a clockwise (anticlockwise) circulation. (b) Heat transport in the Atlantic Ocean (units: PW = 10^{15} W), where the black solid line is the model result averaged from year 520 to year 1031, and the line with red points indicates the values at several sections from the work of Trenberth et al. (2001).

Table 1. The depths and latitudes of AMOC maxima in different models. The models used and listed in Table 1 are different from those in Tables 2 and 3, for reasons explained in the text. The full names of the models are as follows.

Model	Authors	Single or coupled	Depth	Latitude
CCSM3 and CCSM4	Gent et al. (2011)	Coupled	1000 m	near 35°N
CSIRO Mk3L	Phipps et al. (2011)	Coupled	1000 m	30°–60°N
ECHAM-3/LSG	Timmermann et al. (1998)	Coupled	near 1500 m	near 25°N
ECHAM5/MPI-OM	Jungclaus et al. (2005)	Coupled	1000 m	near 30°N
FGOALS-g2	Huang et al. (2014) (present paper)	Coupled	731 m	36.5°N
GFDL Early Version	Delworth et al. (1993)	Coupled	1000–1500 m	45°–50°N
HadCM3	Gordon et al. (2000)	Coupled	800 m	near 40°N
NCEP/GODAS	Huang et al. (2012)	Single	1000 m	near 35°N
NEMO v3.0	Blaker et al. (2012)	Single	1000 m	30°–35°N
IPSL-CM4	Mignot and Frankignoul (2010)	Coupled	1000–1500 m	20°–60°N
UVic ESCM	Rennermalm et al. (2007)	Coupled	1000 m	40°N

CCSM3 and CCSM4: Version 3 and 4 of Community Climate System Model

CSIRO Mk3L: Commonwealth Scientific and Industrial Research Organisation Mark 3 reduced-resolution

ECHAM-3/LSG: European Centre Hamburg Model Version 3/Large Scale Geostrophic

ECHAM5/MPI-OM: European Centre Hamburg Model Version 5/Max Planck Institute ocean model

FGOALS-g2: Flexible Global Ocean–Atmosphere–Land System model, Grid-point Version 2

GFDL Early Version: Geophysical Fluid Dynamics Laboratory Early Version

HadCM3: Hadley Center Model Version 3

NCEP/GODAS: National Centers for Environmental Prediction/Global Ocean Data Assimilation System

NEMO v3.0: Nucleus for European Modelling of the Ocean version 3.0

IPSL-CM4: Institut Pierre Simon Laplace climate model Version 4

UVic ESCM: University of Victoria Earth System Climate Model.

36.8°N, the mean latitude of the 12 models in Table 1.

3.2. The period of AMOC

To locate the source of the decadal signal of AMOC, the period of the AMOC signal at different latitudes of the Atlantic Ocean are analyzed in this section. Zones between 30°S and 60°N in the Atlantic Ocean are evenly divided into six separate regions with a 15° interval, and then the AMOC indices are defined in these six bands in the same way as described in section 2.2. Because the AMOC maximum in FGOALS-g2 locates in the 30°–45°N region, the AMOC index in that region is the same as that defined in 15°–65°N. Spectral analysis was conducted on the time series of the AMOC index of FGOALS-g2 in the above six zones after detrending. From the results (Fig. 3), we may infer that the decadal signal mainly originates from the latitudinal zone 30°–45°N, where the spectrum density of the decadal signal has its maximum. The power spectrum of the AMOC index at 30°–45°N is double-peaked, i.e., one peak at 20 years and another at 32 years.

To further verify the double-peaked periods in AMOC variability according to FGOALS-g2, a wavelet analysis was carried out on the time series of the AMOC index defined in the region 15°–65°N. The results (Fig. 4) show that the double-peaked periods phenomenon is still very obvious in the wavelet power spectrum, i.e., 20 years and 32 years. We could find only one other model in the literature that shows double peaks in the power spectrum of AMOC, and

this is version 3 of the Institute of Numerical Mathematics Climate Model (INMCM3.0), with 16 and 32 years as its peaks (Volodin et al., 2009). An autocorrelation analysis of the AMOC index in FGOALS-g2 revealed that the period of AMOC is 22 years.

Another interesting phenomenon in Fig. 3 is that the decadal signal from the Northern Hemisphere does not pass, or only slightly passes, the Equator. In the region 15°S–15°N, the decadal signal is strongly damped. The conclusion that the Equator acts as a low-pass filter to the decadal and shorter timescale signal by Johnson and Marshall (2002a, b, 2004) and Zhai et al. (2011) is likely reflected in FGOALS-g2, which deserves further investigation using detailed analysis.

3.3. Mean state of convection in the North Atlantic Ocean

The mixed layer depth is a good proxy of the strength and frequency of convection. To calculate the convection index, three regions (red boxes in Figs. 5a and b) defined by Swingedouw et al. (2007) are adopted here to determine the convection sites in a quantitative manner: Region 1—Labrador Sea (48°–66°N, 42°–61°W); Region 2—Irminger Sea (48°–66°N, 42°–10°W); Region 3—GIN Seas, (66°–80°N, 14°W–20°E). Note that the regions do not correspond to the geographic extents of the seas featured in their names, and Region 2 in fact covers a much larger area than the real Irminger Sea. The convection indices for these regions are defined as the area average of mixed layer depth. The observation

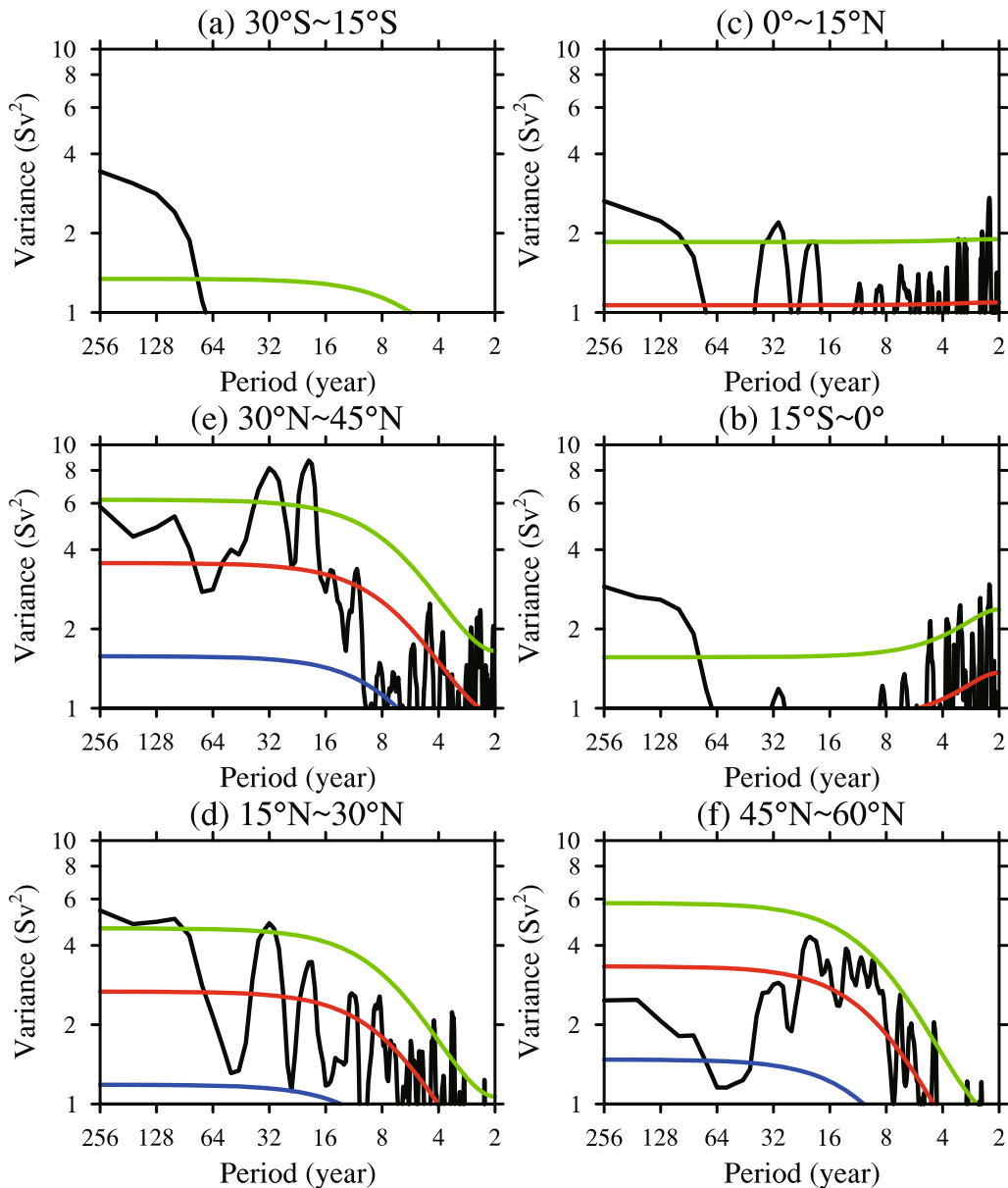


Fig. 3. Power spectrum analysis of the AMOC index, which is defined as the maximum of different latitude bands (shown at the top of each panel). The black solid line is the spectrum density, while the red solid line represents the reference Markov red noise spectrum. The green and blue lines correspond to the 5% and 95% significance levels, respectively.

dataset for mixed layer depth in an annual cycle (12 months) format with a horizontal resolution of 2° is used for comparison (de Boyer Montégut et al., 2004). The estimation of the mixed layer depth is based on a density difference criterion, i.e., the difference between the density at a depth of 10 m and that at the mixed layer depth is 0.03 kg m^{-3} . The data come from the National Oceanographic Data Center and the World Ocean Circulation Experiment database. The data sources used for creating the mixed layer depth include the Mechanical Bathy Thermograph (MBT), eXpendable Bathy Thermograph (XBT), Conductivity-Temperature-Depth (CTD), and Profiling Floats (PFL), which are available since 1941 through 2002.

As illustrated in Figs. 5a and b, the winter (December–April) mixed layer depth in FGOALS-g2 is comparable to the mixed layer depth based on observations. However, the intensity of the simulated deep convection is exaggerated in the Labrador, Irminger and GIN Seas, although the maximum intensity in the GIN Seas is underestimated. The annual cycles of the convection indices in the three defined regions are simulated well (see Figs. 5c and d). Also, the overestimated convection in wintertime in the above three regions is more obvious in Figs. 5c and d, which is partially caused by the high background vertical mixing coefficient at these locations. Vertical mixing should be very strong when the Richardson number is very small. However, a bug in the

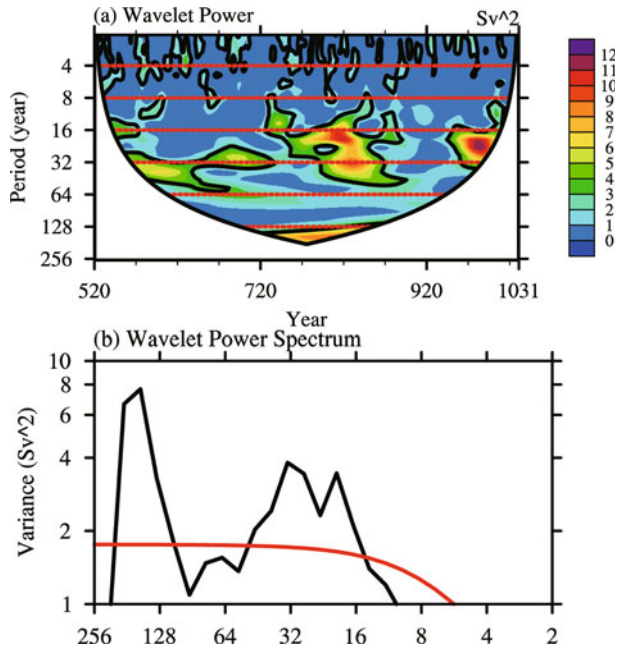


Fig. 4. Wavelet analysis of the AMOC index, which is defined as the maximum from 15°N to 65°N and below 500 m depth. (a) Wavelet power; (b) wavelet power spectrum, in which the black solid line is the spectrum density and the red solid line represents the reference Markov red noise spectrum.

vertical interpolation process before running the vertical mixing scheme of LICOM2.0 leads to weak vertical mixing. To overcome this problem, a high background vertical mixing coefficient is taken.

3.4. Region of convection with strongest connection to AMOC

This subsection is devoted to identifying the region in which convection is most strongly related to the decadal variability of AMOC.

Figure 6 shows the first two empirical orthogonal function (EOF) modes of simulated winter (December–April) mixed layer depth by FGOALS-g2 for 512 years. The first mode (Fig. 6a) explains about 28% of the total variance, shows pronounced decadal variability against the red noise background (Fig. 6c) and has its center of action in the Labrador Sea with an amplitude of about 260 m (Fig. 6a). The second mode (Fig. 6d), which has its center of action in the GIN Seas with an amplitude of about 156 m, explains only about 12% of the total variance. The time evolution of this mode shows very little decadal variability, but more variability on multi-centennial timescales than the first mode (Fig. 6f). Therefore, the decadal AMOC variability may be more strongly connected to the convective variability in the Labrador Sea, while multi-centennial AMOC variability may be more connected to the GIN Seas. This phenomenon has also been found in a CO₂ doubling experiment using the same model (Huang et

al., 2013).

A lag correlation analysis was performed between the AMOC index and the three convection indices defined in the above three regions, and the results are shown in Fig. 7. As can be seen, the Labrador Sea convection in FGOALS-g2 leads AMOC by three years with a high correlation coefficient of 0.61, while the Irminger Sea convection leads AMOC by five years with a weak correlation of 0.21. The convection in the GIN Seas leads AMOC by nine years with a weak correlation of 0.3. Possible explanations for the longer time lag and weaker correlation for the GIN Seas than that for the Labrador Sea are: (1) the deep water formed in the GIN Seas needs to move southward into the Irminger Sea or Labrador Sea to form the deep water branch of AMOC (see the position of the deep water branch of AMOC in Fig. 2a); (2) the relatively shallow Greenland-Scotland Ridge is separating the subpolar region of the North Atlantic Ocean and GIN Seas, preventing the deep water in the GIN Seas to directly enter the subpolar region of the North Atlantic Ocean, which was suggested by a study using the new version of the BCM model (Medhaug et al., 2012). Thus, the deep convection in the Labrador Sea is closely related to the strength of AMOC.

3.5. The effects of salinity and temperature on AMOC variability

Since changes in the deep convection are mainly attributed to upper ocean density changes (we refer here to the upper 250 m in the ocean model), we split the contributions of temperature and salinity to density according to Delworth et al. (1993), Krebs and Timmermann (2007), and Swingedouw et al. (2007), which can be formulated as

$$d\rho = -\alpha dT + \beta dS, \tag{1}$$

where ρ is the ocean density, T is the potential temperature, S is the salinity, and α and β are the thermal expansion and haline contraction coefficients. The thermal and haline contributions to the upper ocean density changes in these regions are shown in Fig. 8. It is clear that the upper ocean density changes in the Labrador and Irminger Seas are mainly caused by temperature changes, and those in the GIN Seas are due to salinity changes. However, observations reveal a different picture in the GIN Seas, i.e., the formation of dense water that spills over the Greenland-Scotland Ridge is mainly attributed to heat loss of the northward flow carrying warm Atlantic Water (Eldevik et al., 2009). In FGOALS-g2, the annual means of temperature and salinity in the GIN Seas are 1.83°C and 35.27 psu, while those in the Labrador Sea are 5.81°C and 35.39 psu. Thus, the GIN Seas have a much lower thermal expansion coefficient than that of the Labrador Sea, which is the reason for the salinity-dominant density changes in the GIN Seas. The role of thermal effects on deep convection in the Labrador and Irminger Seas in FGOALS-g2 compares well with observations, which emphasizes the effect of heat loss on convection in winter (Marshall and Schott, 1999; Steffen and D’Asaro, 2002; Yashayaev et al., 2007).

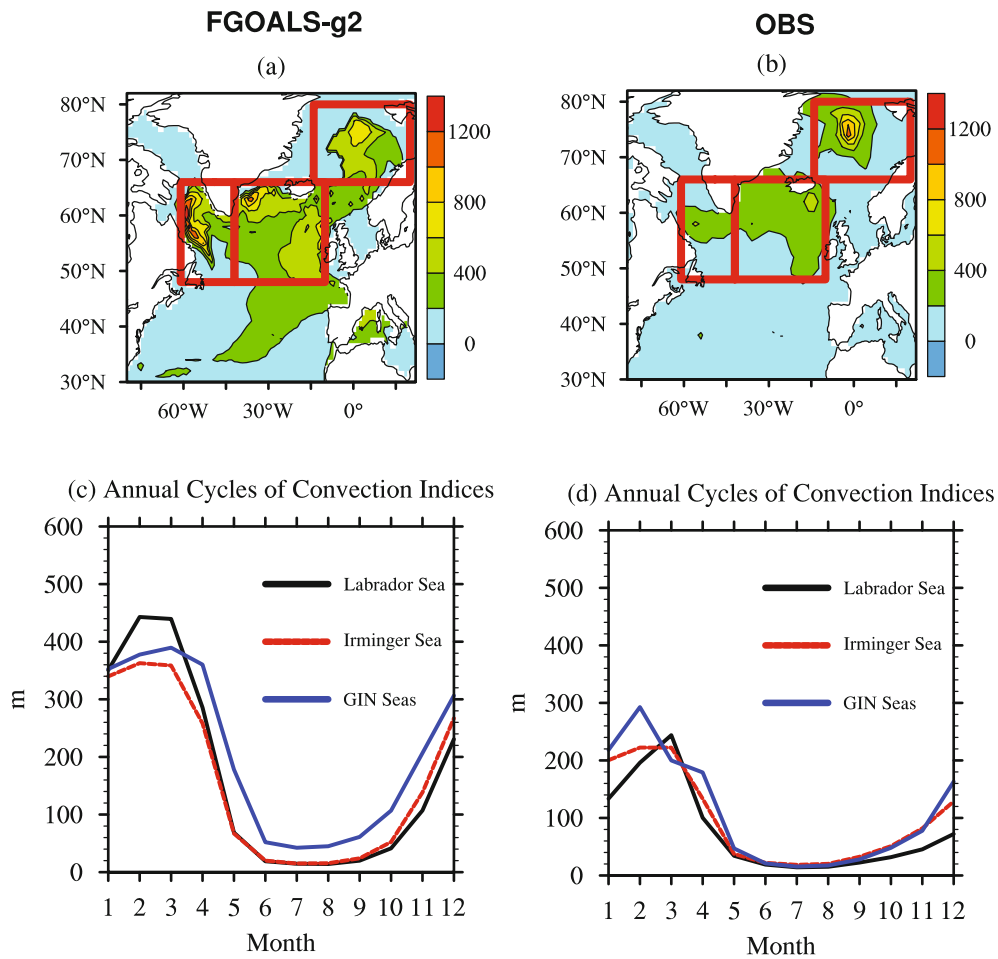


Fig. 5. Winter mixed layer depth (units: m) of (a) FGOALS-g2 and (b) observations (de Boyer Montégut et al, 2004). (c, d) Annual cycles of the convection indices for FGOALS-g2 and observations, respectively. The convection indices in (c) and (d) are defined in the three boxes shown in (a) and (b) (see section 3.3 for the definitions of the three seas). The mixed layer depth of FGOALS-g2 in (a) is constructed using the data from December to April of the 512-yr period. The observed mixed layer depth is given in 12-month format, and the five months have been averaged.

3.6. Regression analysis

A regression analysis was carried out in such a way that all the time series of the spatial patterns of potential temperature, salinity, and the eastward and northward velocity components averaged in the upper 250 m were regressed onto the time series of the AMOC index (Fig. 9).

Several years (3–4) before an increase in AMOC, the temperature of the upper Labrador Sea decreases. The negative temperature anomaly has two direct influences: (1) generating a cyclonic current anomaly, further speeding up the background currents, i.e., the subpolar gyre, which is a cyclonic current; and (2) increasing the density in the Labrador Sea and promoting deep water formation there. The collective consequence of these two direct influences is to speed up AMOC, which will be at its maximum with a 3–4-yr time lag. In turn, the strengthening of AMOC increases the temperature of the Labrador Sea with a time lag. Combining the results from Figs. 8a and 9, this time lag is about 7–8 years.

Therefore, 11 years are needed to complete a temperature reversal in the Labrador Sea, which means the period for the full cycle of the “damped oscillation” is about 22 years. It should be noted that the above mechanism is very similar to that of Lohmann et al. (2009) based on results from the Miami Isopycnic Coordinate Ocean Model (MICOM).

4. Characteristics of AMOC variability in different models

In this section, characteristics of AMOC variability according to 12 different models, including FGOALS-g2, are compared using the results from previously published studies (see Table 2 for details). Each of these 12 models satisfies two requirements: 1) the model must be a coupled climate model; and 2) the period of AMOC for the model must have been analyzed. It should be noted that the models used here (see Tables 2 and 3) are different from those used for eval-

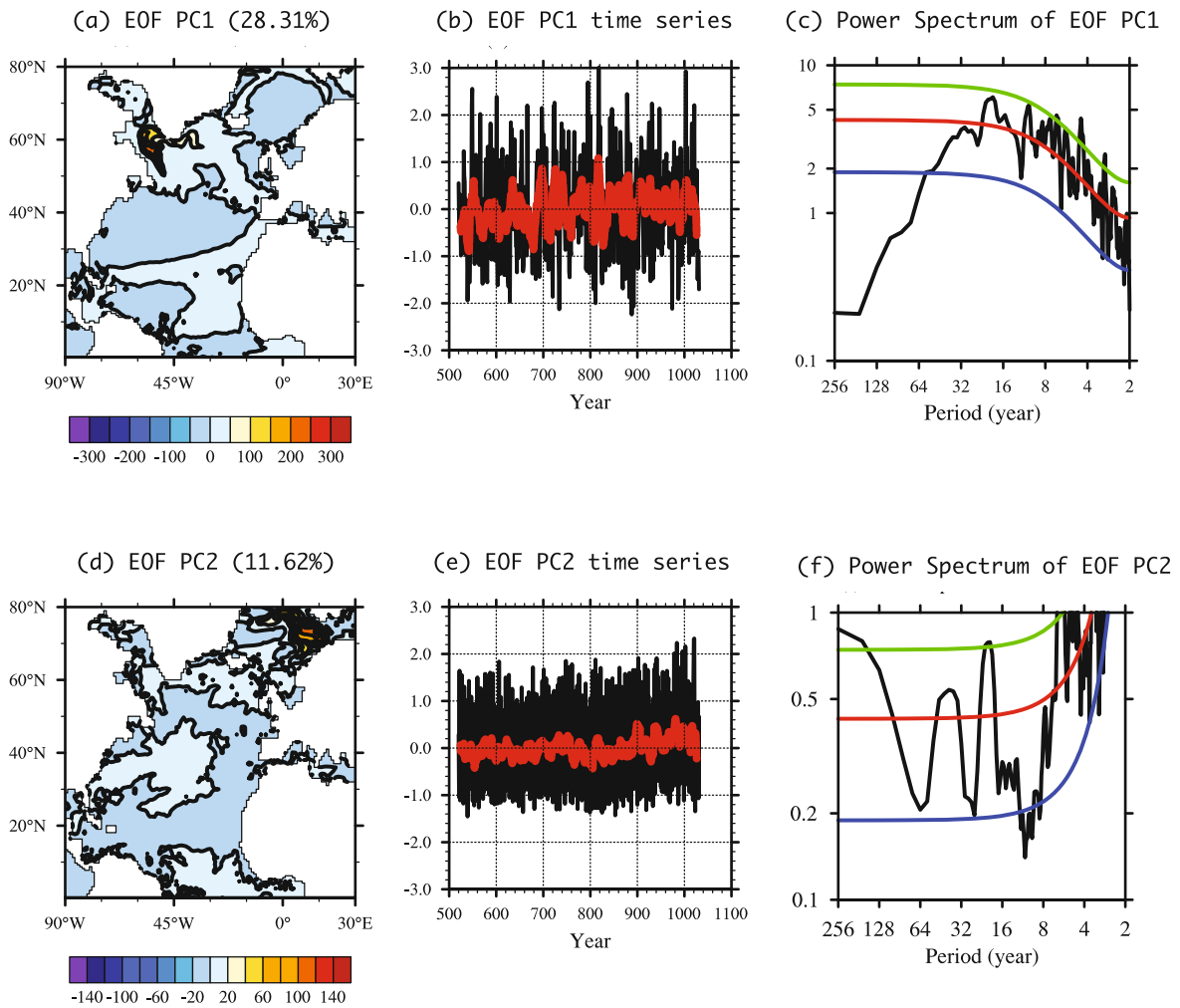


Fig. 6. The first and second modes of winter mixed layer depths from year 520 to 1031 after EOF analysis was carried out for the region (0°–80°N, 90°W–30°E). (a–c) First mode, normalized time series of the first mode, and power spectrum of the first-mode normalized time series, respectively. (d–f) The same as (a–c), but for the second mode. In (b) and (e), the black solid line is the unsmoothed time series and the red dashed line is a 10-yr running average of the normalized time series. In (c) and (f), the black solid line is the spectrum density, the red solid line indicates the reference Markov red noise spectrum, and the green and blue lines correspond to the 5% and 95% significance levels, respectively.

uating the mean state of AMOC (see Table 1). The periods of AMOC, regions of convection with strongest connection to AMOC, and the time lags between AMOC and the convection for the 12 models are also given in Table 2. The main contributor (thermal or haline effect) to changes in the upper ocean densities in the convective regions and the time lags between AMOC and the thermal and haline effects are given in Table 3. It should be noted that uncertainties exist when comparing the relative contributions of temperature or salinity changes to the upper ocean density using the results reported in different studies: (1) the definition of the upper ocean varies, ranging from the upper 200 to the upper 300 m; (2) systematic biases of temperature and salinity in different models are not the same, and thus the choices of both the thermal expansion and haline contraction coefficients can be somewhat subjective; and (3) the regions of convection may

be defined in different ways from one model to another.

It is suggested from the information presented in Table 2 that the periods of AMOC for different coupled climate models are widespread, ranging from 20 to more than 100 years. The Labrador Sea is the region of convection with strongest connection to AMOC in nearly all the models except the HadCM3 model (Dong and Sutton, 2005). As noted by Bailey et al. (2005), the dominant role of the Labrador Sea in AMOC variability in many climate models can be partially attributed to the weak or diluted GIN Seas overflow in these models. It is interesting that the CCSM4 model has a wide spectrum of low frequency oscillation covering the 50–200-yr range. In contrast, the previous version, CCSM3, only has a period of 21 years. However, this longer timescale of AMOC variability in CCSM4 has not been explained (Danabasoglu et al., 2012). NorESM1-M (Bentsen et al., 2012) and BCM

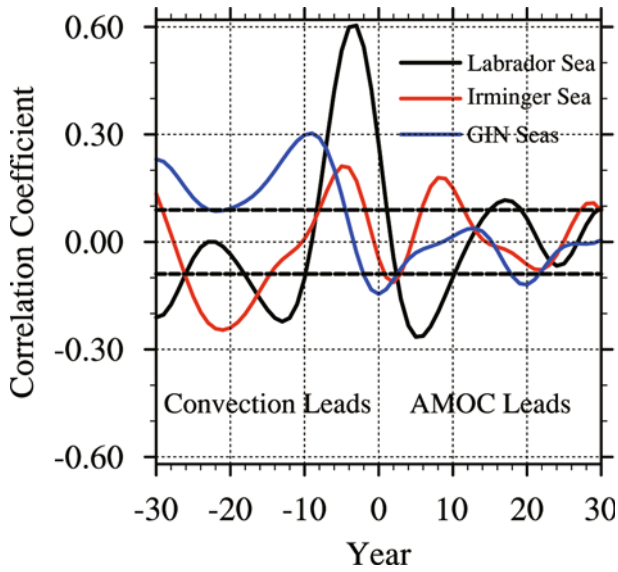


Fig. 7. Correlations of AMOC and the convection indices in the three different regions. A positive (negative) N year in the x -axis means AMOC leads (lags) the convection by N years. The convection indices are constructed using the area average of the mixed layer depth from December to April. The black, red and blue solid lines correspond to the Labrador Sea, Irminger Sea and the GIN Seas, respectively. The black dashed lines represent the 5% significance level using 480 as the degrees of freedom, obtained using a two-sided Student's t -test.

(Bentsen et al., 2004), sharing the same ocean component (MICOM), have the same period of 20 years. However, timescales of AMOC variability in an updated version of BCM range from 40 to 70 years, and the Labrador Sea and GIN Seas overflow produce 1/3 and 2/3 of NADW, respectively (Medhaug et al., 2012). In general, across all the models, AMOC peaks arrive less than 5 years after the peaks of convection. There is one exception, ECHAM5/MPI-OM (Jungclaus et al., 2005), in which the AMOC peaks arrive 12 years after the peaks of convection.

It is suggested by many coupled climate models that the density anomalies in the convective regions or the sinking regions are very critical to deep-water formation and, furthermore, the strength of AMOC. However, the contributions of thermal and haline effects to the density anomalies in the upper ocean diverge in different coupled climate models (Table 3).

As shown in Table 3, salinity plays a dominant role in regulating the upper ocean density of the Labrador Sea in CCSM4 (Danabasoglu et al., 2012) and that of the GIN Seas in HadCM3 (Dong and Sutton, 2005). In addition, the period of AMOC in CCSM4 is 50–200 years (Danabasoglu et al., 2012), which is longer than that found in the other models. The dominant role of salinity in HadCM3 can be attributed to a different convective region (GIN Seas, Irminger Sea) with the strongest connection to AMOC: the GIN Seas are colder than the Labrador Sea and thus have a lower thermal expansion.

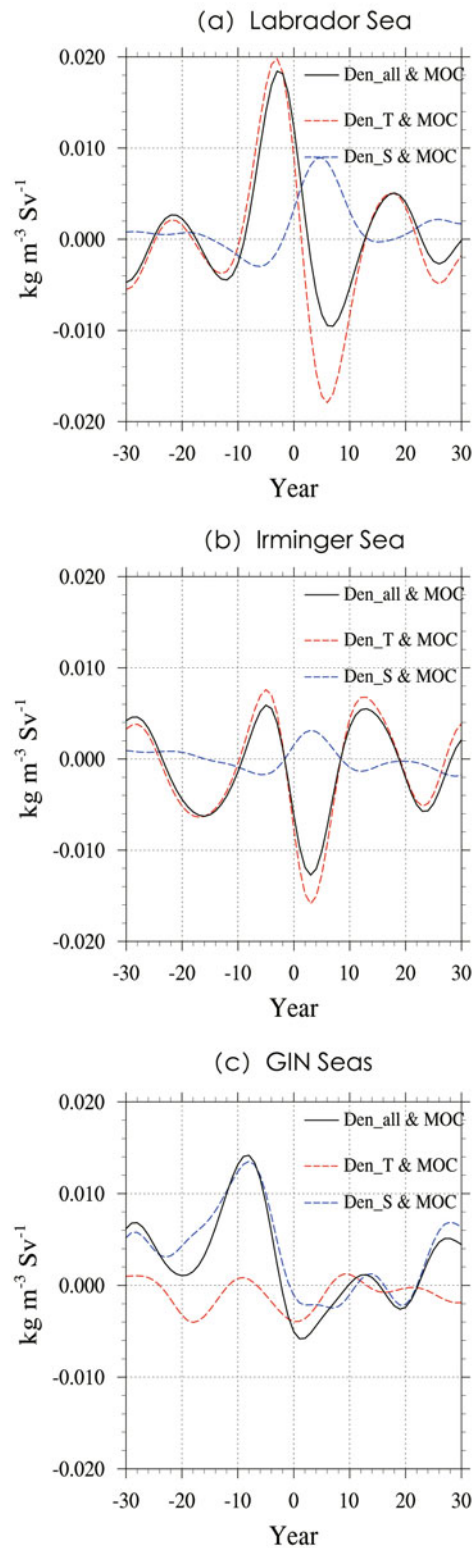


Fig. 8. Density time series regressions onto the AMOC index time series. (a–c) Labrador Sea, Irminger Sea and GIN Seas, respectively. A positive (negative) N year in the x -axis means AMOC leads (lags) the density by N years. The black solid line represents the total density. The red and blue dashed lines represent the thermal and haline contributions to the total density, respectively.

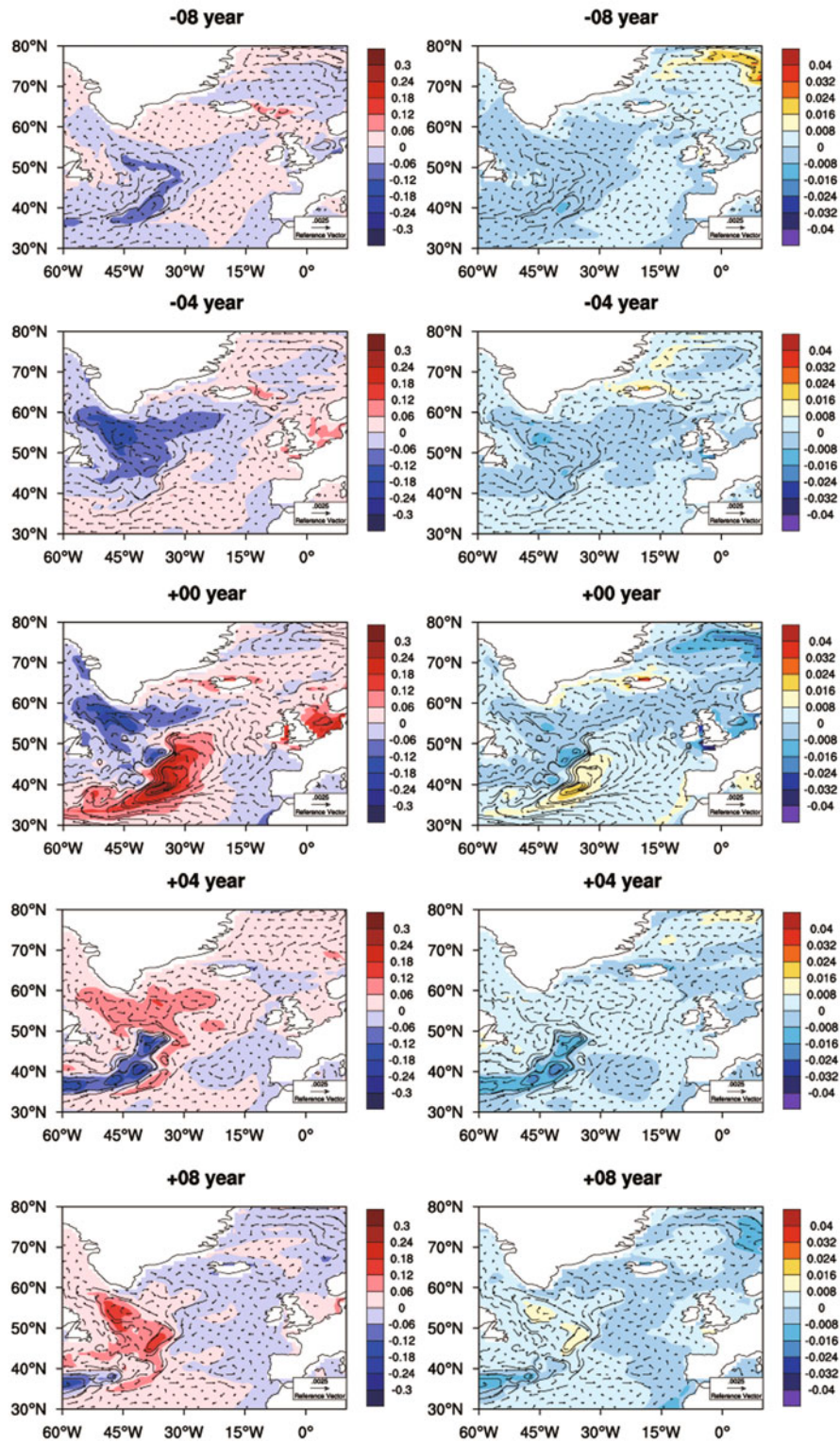


Fig. 9. Lag regressions between the AMOC index and the potential temperature, salinity and velocity averaged in the upper 250 m of the North Atlantic Ocean. The colored regions in the left panels show the regressions between the AMOC index and potential temperature (units: $^{\circ}\text{C Sv}^{-1}$), while the colored regions in the right panels show the regressions between the AMOC index and salinity (units: psu Sv^{-1}). In all the panels, the vectors draw the regressions of the AMOC index and velocity (units: $\text{m s}^{-1} \text{Sv}^{-1}$). A positive (negative) year at the top of each panel means AMOC leads (lags) the other fields by several years. To obtain the regression between the AMOC index and the velocity, two regressions were carried out between the AMOC index and the two velocity components, i.e., the northward and eastward components.

Table 2. The periods of AMOC, the convective regions with the strongest connection to AMOC, and the years the convection leads AMOC in 12 coupled climate models. The contributions of ECHAM-3/LSG and GFDL Early Version are calculated in the sinking region (45° – 65° N and 52° – 72° N, respectively). The models used and listed in Tables 2 and 3 are different from those in Table 1, for reasons explained in the text. Most of the model names can be referred to Table 1.

Model	Authors	Period	Convection	Convection lead
Updated version of BCM	Medhaug et al. (2012)	40–70 years	Labrador Sea	2 years
BCM	Bentsen et al. (2004)	20 years	Labrador Sea and Irminger Sea	2–5 years
CCSM3	Danabasoglu (2008)	21 years	Labrador Sea	5 years
CCSM4	Danabasoglu et al. (2012)	50–200 years	Labrador Sea	2 years
ECHAM-3/LSG	Timmermann et al. (1998)	35 years	Sinking region	5 years
ECHAM5/MPI-OM	Jungclaus et al. (2005)	70–80 years	Labrador Sea	12 years
FGOALS-g2	Huang et al. (2014) (present paper)	22 years	Labrador Sea	3–4 years
GFDL Early Version	Delworth et al. (1993)	50 years	Sinking region	4 years
HadCM3	Dong and Sutton (2008)	25 years	GIN Seas and Irminger Sea	4 years
INMCM3.0	Volodin et al. (2009)	16–32 years	Not given	Not given
IPSL-CM5	Escudier et al. (2011)	20 years	Not given	Not given
NorESM1-M	Bentsen et al. (2012)	20 years	Not given	Not given

BCM: Bergen Climate Model, INMCM3.0: Institute for Numerical Mathematics Climate Model Version 3.0, and NorESM1-M: Norwegian Earth System Model Version 1-Medium Resolution.

Table 3. Contributions of temperature and salinity changes to the upper ocean density of the convective regions with the strongest connection to AMOC, or the sinking regions, which are given in Table 2 for the 12 coupled climate models. The number of years that thermal and haline contributions lead AMOC changes are also given. Five levels are used to qualitatively describe the relative importance of thermal and saline effects, i.e. “salinity-dominated”, “salinity more”, “both”, “temperature more”, and “temperature-dominated”, which correspond to the contribution of salinity changes being more than 85%, between 85% and 65%, between 65% and 35%, between 35% and 15%, and less than 15% to the density changes in the upper ocean, respectively. The models used and listed in Tables 3 and 2 are different from those in Table 1, for reasons explained in the text.

Model	Contribution	Thermal lead	Salinity lead
Updated version of BCM	Not given	Not given	Not given
BCM	Not given	Not given	Not given
CCSM3	Both	2 years	4 years
CCSM4	Salinity-dominated	Not given	2–3 years
ECHAM-3/LSG	Salinity more	8 years	1–2 years
ECHAM5/MPI-OM	Salinity more	40 years	0 years
FGOALS-g2	Temperature-dominated	3–4 years	–4 years
GFDL Early Version	Salinity more	7 years	–2 years
HadCM3	Salinity-dominated	Not given	4 years
INMCM3.0	Not given	Not given	Not given
IPSL-CM5	Not given	Not given	Not given
NorESM1-M	Not given	Not given	Not given

Salinity plays a more important role than temperature in modulating the density in the upper ocean of the sinking region in ECHAM-3/LSG (AMOC period of 35 years) (Timmermann et al., 1998), and the sinking region of the GFDL Early Version (AMOC period of 50 years) (Delworth et al., 1993) and the Labrador Sea in ECHAM5/MPI-OM (AMOC period of 70–80 years) (Jungclaus et al., 2005). The colder GIN Seas included in the sinking region are also the reason for salinity contributing more in the GFDL model (Delworth et al., 1993).

When the periods of AMOC are short (around 20 years) and the convective region with the strongest connection to AMOC is the Labrador Sea, the thermal contribution is more obvious (CCSM3 and FGOALS-g2). However, in CCSM3 the positive density anomalies induced by salinity changes

occur before those induced by temperature changes (Danabasoglu, 2008), which is different from FGOALS-g2. Interestingly, in BCM (AMOC period of 20 years), the convective characteristics in the three regions are very similar to FGOALS-g2: the convection of the Labrador and GIN Seas are in opposite phase, while that in the Irminger Sea is in-phase or leads the Labrador Sea (see Fig. 7 for FGOALS-g2).

In the models whose convective region with the strongest connection to AMOC is the Labrador Sea, we can conclude that AMOC variability can be attributed to more salinity changes for longer periods (longer than 35 years) and to more temperature changes for shorter periods. In four of the models (see Table 3), i.e., ECHAM3/LSG, ECHAM5-MPI-OM, FGOALS-g2 and GFDL Early Version, it is found that the thermal contributions to the density changes in the upper

ocean lead the haline contributions by several years.

5. Summary and conclusions

A new method to determine the most stable state of the long-term (1500-yr) pre-industrial control experiment by FGOALS-g2 was developed based on the minimum SD of a running time window of the AMOC index, and the only adjustable parameter was the length of the time window. Using this new method, and setting the length of the time window to 512 years, the initial spin-up and final long-term climate drift periods were removed, and the corresponding linear tendencies of AMOC indices in these two periods were -2.1×10^{-3} and -1.8×10^{-3} Sv yr⁻¹, respectively. The 512-year window with a linear tendency of the AMOC index of about 8.5×10^{-6} Sv yr⁻¹ was selected to study the internal variability of AMOC.

Using spectral and wavelet analysis, a double-peak was found in the AMOC spectrum of FGOALS-g2 with periods of 20 and 32 years, while an autocorrelation analysis suggested a period of 22 years. Associated mechanisms have been investigated in this paper. The convective region with the strongest connection to AMOC variability in FGOALS-g2 is the Labrador Sea. The deep convection in the Labrador Sea of FGOALS-g2 is closely related to the temperature changes at this site. A positive density anomaly generated by the negative temperature anomaly in the Labrador Sea leads an AMOC strengthening after 3–4 years. The AMOC strengthening, in turn, leads a warming of the Labrador Sea after another 7–8 years. Thus, a temperature reversal in the Labrador Sea occurs after 11 years, which gives a time of 22 years for the full cycle of the “damped oscillation”.

From a comparison of 12 coupled climate models, it was found that when the convective region with the strongest connection to AMOC is the Labrador Sea, AMOC variability with a longer period can be mainly attributed to salinity changes, and that with a shorter period to temperature changes.

Acknowledgements. The authors sincerely thank the two anonymous reviewers for their valuable comments, which led to the present improved version of the original manuscript. A discussion with ZHANG Xuehong and LIU Hailong was extremely helpful. This work was supported by the Ministry of Science and Technology of China for the National High-tech R&D Program (863 Program; Grant No. 2010AA012304), the National Basic Research Program of China (973 Program; Grant Nos. 2011CB309704 and 2010CB951904), and the National Natural Science Foundation of China (Grant Nos. 41023002 and 41005053).

REFERENCES

- Bailey, D., P. Rhines, and S. Häkkinen, 2005: Formation and pathways of North Atlantic deep water in a coupled ice-ocean model of the Arctic-North Atlantic Oceans. *Climate Dyn.*, **25**, 497–516.
- Bentsen, M., H. Drange, T. Furevik, and T. Zhou, 2004: Simulated variability of the Atlantic meridional overturning circulation. *Climate Dyn.*, **22**(6), 701–720, doi: 10.1007/s00382-004-0397-x.
- Bentsen, M., and Coauthors, 2012: The Norwegian earth system model, NorESM1-M - Part 1: Description and basic evaluation. *Geoscientific Model Development Discussion*, **5**, 2843–2931.
- Blaker, A. T., Joël J-M Hirschi, B. Sinha, B. de Cuevas, S. Alderson, A. Coward, and G. Madec, 2012: Large near-inertial oscillations of the Atlantic meridional overturning circulation. *Ocean Modelling*, **42**, 50–56.
- Bryden, H. L., and S. Imawaki, 2001: Ocean heat transport. *Ocean Circulation & Climate: Observing and Modelling the Global Ocean*, G. Siedler et al., Eds., Academic Press, San Diego, San Francisco, New York, Boston, London, Sydney, Tokyo, 455–474.
- Canuto, V. M., A. Howard, Y. Cheng, and M. S. Dubovikov, 2001: Ocean turbulence. Part I: One-point closure model—momentum and heat vertical diffusivities. *J. Phys. Oceanogr.*, **31**(6), 1413–1426.
- Canuto, V. M., A. Howard, Y. Cheng, and M. S. Dubovikov, 2002: Ocean turbulence. Part II: Vertical diffusivities of momentum, heat, salt, mass, and passive scalars. *J. Phys. Oceanogr.*, **32**(1), 240–264.
- Craig, A. P., and Coauthors, 2005: CPL6, The new extensible, high performance parallel coupler for the community climate system. *International Journal of High Performance Computing Application*, **19**, 308–327.
- Cunningham, S. A., and Coauthors, 2007: Temporal variability of the Atlantic meridional overturning circulation at 26.5°N. *Science*, **317**(5840), 935–938, doi: 10.1126/science.1141304.
- Danabasoglu, G., 2008: On multidecadal variability of the Atlantic meridional overturning circulation in the community climate system model version 3. *J. Climate*, **21**, 5524–5544, doi: 10.1175/2008jcli2019.1.
- Danabasoglu, G., S. G. Yeager, Y.-O. Kwon, J. J. Tribbia, A. S. Phillips, and J. W. Hurrell, 2012: Variability of the Atlantic meridional overturning circulation in CCSM4. *J. Climate*, doi: 10.1175/jcli-d-11-00463.1.
- de Boyer Montégut, C., G. Madec, A. S. Fischer, A. Lazar, and D. Iudicone, 2004: Mixed layer depth over the global ocean: An examination of profile data and a profile-based climatology. *J. Geophys. Res.*, **109**(C12), C12003, doi: 10.1029/2004jc002378.
- Delworth, T., S. Manabe, and R. J. Stouffer, 1993: Interdecadal variations of the thermohaline circulation in a coupled ocean-atmosphere model. *J. Climate*, **6**(11), 1993–2011.
- Delworth, T. L., and M. E. Mann, 2000: Observed and simulated multidecadal variability in the Northern Hemisphere. *Climate Dyn.*, **16**(9), 661–676, doi: 10.1007/s003820000075.
- Delworth, T. L., and Coauthors, 2006: GFDL's CM2 global coupled climate models. Part I: Formulation and simulation characteristics. *J. Climate*, **19**(5), 643–674, doi: 10.1175/jcli3629.1.
- Delworth, T. L., and Coauthors, 2008: The potential for abrupt change in the Atlantic Meridional Overturning Circulation. *Abrupt Climate Change*. A report by the U.S. Climate Change Science Program and the Subcommittee on Global Change Research. U.S. Geological Survey, Reston, VA, 258–359.
- Doney, S. C., K. Lindsay, I. Fung, and J. John, 2006: Natural variability in a stable, 1000-Yr global coupled climate-carbon cycle simulation. *J. Climate*, **19**(13), 3033–3054, doi:

- 10.1175/jcli3783.1.
- Dong, B., and R. T. Sutton, 2005: Mechanism of interdecadal thermohaline circulation variability in a coupled ocean-atmosphere GCM. *J. Climate*, **18**(8), 1117–1135, doi: 10.1175/jcli3328.1.
- Döös, K., and D. J. Webb, 1994: The deacon cell and the other meridional cells of the southern ocean. *J. Phys. Oceanogr.*, **24**(2), 429–442.
- Dufour, C. O., J. L. Sommer, J. D. Zika, M. Gehlen, J. C. Orr, P. Mathiot, and B. Barnier, 2012: Standing and transient eddies in the response of the meridional overturning to the southern annular mode. *J. Climate*, **25**, 6958–6974.
- Eldevik, T., J. E. Ø. Nilssen, D. Iovino, K. A. Olsson, A. B. Sandø, and H. Drange, 2009: Observed sources and variability of Nordic seas overflow. *Nature Geoscience*, **2**(6), 406–410.
- Escudier, R., J. Mignot, and D. Swingedouw, 2011: A 20-yr coupled ocean-sea ice-atmosphere variability mode in the North Atlantic in an AOGCM. *Climate Dyn.*, **40**, 619–636.
- Gent, P. R., and Coauthors, 2011: The community climate system model version 4. *J. Climate*, **24**(19), 4973–4991, doi: 10.1175/2011jcli4083.1.
- Gordon, A. L., 2009: Bottom Water Formation, in *Ocean Currents*. J. H. Steele et al., Eds., Elsevier, London, 263–269.
- Gordon, C., and Coauthors, 2000: The simulation of SST, sea ice extents and ocean heat transports in a version of the Hadley centre coupled model without flux adjustments. *Climate Dyn.*, **16**(2), 147–168, doi: 10.1007/s003820050010.
- Hansen, B., W. R. Turrell, and S. Østerhus, 2001: Decreasing overflow from the Nordic seas into the Atlantic Ocean through the Faroe Bank channel since 1950. *Nature*, **411**, 927–930.
- Hofmann, M., and S. Rahmstorf, 2009: On the stability of the Atlantic meridional overturning circulation. *PNAS*, **106**(49), 20584–20589.
- Huang, B., Y. Xue, A. Kumar, and D. Behringer, 2012: AMOC variations in 1979–2008 simulated by NCEP operational ocean data assimilation system. *Climate Dyn.*, **38**(3), 513–525, doi: 10.1007/s00382-011-1035-z.
- Huang, W. Y., and Coauthors, 2013: Understanding the different responses of Atlantic meridional overturning circulation (AMOC) under the three representative concentration pathways (RCPs) in FGOALS-g2. *Climatic and Environmental Research*, in press. (in Chinese)
- Johns, W. E., and Coauthors, 2011: Continuous, array-based estimates of Atlantic Ocean heat transport at 26.5°N. *J. Climate*, **24**(10), 2429–2449, doi: 10.1175/2010jcli3997.1.
- Johnson, H. L., and D. P. Marshall, 2002a: A theory for the surface atlantic response to thermohaline variability. *J. Phys. Oceanogr.*, **32**(4), 1121–1132.
- Johnson, H. L., and D. P. Marshall, 2002b: Localization of abrupt change in the North Atlantic thermohaline circulation. *Geophys. Res. Lett.*, **29**(6), 1083, doi: 10.1029/2001gl014140.
- Johnson, H. L., and D. P. Marshall, 2004: Global teleconnections of meridional overturning circulation anomalies. *J. Phys. Oceanogr.*, **34**(7), 1702–1722.
- Jungclaus, J. H., H. Haak, M. Latif, and U. Mikolajewicz, 2005: Arctic-North Atlantic interactions and multidecadal variability of the meridional overturning circulation. *J. Climate*, **18**(19), 4013–4031, doi: 10.1175/jcli3462.1.
- Kanzow, T., and Coauthors, 2009: Basinwide integrated volume transports in an eddy-filled ocean. *J. Phys. Oceanogr.*, **39**(12), 3091–3110, doi: 10.1175/2009jpo4185.1.
- Kanzow, T., and Coauthors, 2010: Seasonal Variability of the Atlantic Meridional Overturning Circulation at 26.5°N. *J. Climate*, **23**(21), 5678–5698, doi: 10.1175/2010jcli3389.1.
- Knight, J. R., R. J. Allan, C. K. Folland, M. Vellinga, and M. E. Mann, 2005: A signature of persistent natural thermohaline circulation cycles in observed climate. *Geophys. Res. Lett.*, **32**(20), L20708, doi: 10.1029/2005gl024233.
- Krebs, U., and A. Timmermann, 2007: Fast advective recovery of the Atlantic meridional overturning circulation after a Heinrich event. *Paleoceanography*, **22**(1), PA1220, doi: 10.1029/2005pa001259.
- Kuhlbrodt, T., A. Griesel, M. Montoya, A. Levermann, M. Hofmann, and S. Rahmstorf, 2007: On the driving processes of the Atlantic meridional overturning circulation. *Rev. Geophys.*, **45**, RG2001, doi:10.1029/2004RG000166.
- Kwon, Y.-O., and C. Frankignoul, 2012: Stochastically-driven multidecadal variability of the Atlantic meridional overturning circulation in CCSM3. *Climate Dyn.*, **38**(5), 859–876, doi: 10.1007/s00382-011-1040-2.
- Latif, M., and N. S. Keenlyside, 2011: A perspective on decadal climate variability and predictability. *Deep Sea Research Part II: Topical Studies in Oceanography*, **58**, 1880–1894, doi: 10.1016/j.dsr2.2010.10.066.
- Latif, M., and Coauthors, 2004: Reconstructing, monitoring, and predicting multidecadal-scale changes in the North Atlantic thermohaline circulation with sea surface temperature. *J. Climate*, **17**, 1605–1614.
- Li, L. J., and Coauthors, 2013a: The flexible global ocean-atmosphere-land system model: Version g2: FGOALS-g2. *Adv. Atmos. Sci.*, **30**(3), 543–560, doi: 10.1007/s00376-012-2140-6.
- Li, L. J., and Coauthors, 2013b: Development and evaluation of grid-point atmospheric model of IAP LASG, Version 2.0 (GAMIL 2.0). *Adv. Atmos. Sci.*, **30**(3), 855–867, doi: 10.1007/s00376-013-2157-5.
- Liu, H., P. Lin, Y. Yu, and X. Zhang, 2012: The baseline evaluation of LASG/IAP climate system ocean model (LICOM) version 2. *Acta Meteorologica Sinica*, **26**(3), 318–329, doi: 10.1007/s13351-012-0305-y.
- Liu, J., 2010: Sensitivity of sea ice and ocean simulations to sea ice salinity in a coupled global climate model. *Science China: Earth Science*, **53**(6), 911–918, doi: 10.1007/s11430-010-0051-x.
- Lohmann, K., H. Drange, and M. Bentsen, 2009: Response of the North Atlantic subpolar gyre to persistent North Atlantic oscillation like forcing. *Climate Dyn.*, **32**, 273–285.
- Mahajan, S., R. Zhang, and T. L. Delworth, 2011: Impact of the Atlantic meridional overturning circulation (AMOC) on Arctic surface air temperature and sea ice variability. *J. Climate*, **24**, 6573–6581, doi: 10.1175/2011jcli4002.1.
- Marshall, J., and F. Schott, 1999: Open-ocean convection: Observations, theory, and models. *Rev. Geophys.*, **37**, 1–64, doi: 10.1029/98rg02739.
- Medhaug, I., and T. Furevik, 2011: North Atlantic 20th century multidecadal variability in coupled climate models: Sea surface temperature and ocean overturning circulation. *Ocean Science*, **7**(3), 389–404, doi: 10.5194/os-7-389-2011.
- Medhaug, I., H. Langehaug, T. Eldevik, T. Furevik, and M. Bentsen, 2012: Mechanisms for decadal scale variability in a simulated Atlantic meridional overturning circulation. *Climate Dyn.*, **39**, 77–93, doi: 10.1007/s00382-011-1124-z.
- Mignot, J., and C. Frankignoul, 2010: Local and remote impacts of a tropical Atlantic salinity anomaly. *Climate Dyn.*, **35**(7),

- 1133–1147, doi: 10.1007/s00382-009-0621-9.
- Oleson, K. W. and Coauthors, 2004: Technical description of the community land model (CLM). NCAR/TN-461+STR, 174 pp.
- Otterå, O. H., M. Bentsen, H. Drange, and L. Suo, 2010: External forcing as a metronome for Atlantic multidecadal variability. *Nature Geoscience*, **3**(10), 688–694.
- Pacanowski, R. C., and S. G. H. Philander, 1981: Parameterization of vertical mixing in numerical models of tropical oceans. *J. Phys. Oceanogr.*, **11**, 1443–1451.
- Phipps, S. J., L. D. Rotstayn, H. B. Gordon, J. L. Roberts, A. C. Hirst, and W. F. Budd, 2011: The CSIRO Mk3L climate system model version 1.0—Part 1: Description and evaluation. *Geoscience Model Development Discussion*, **4**(1), 219–287, doi: 10.5194/gmdd-4-219-2011.
- Rennermalm, A. K., E. F. Wood, A. J. Weaver, M. Eby, and S. J. Déry, 2007: Relative sensitivity of the Atlantic meridional overturning circulation to river discharge into Hudson Bay and the Arctic Ocean. *J. Geophys. Res.*, **112**(G4), G04S48, doi: 10.1029/2006jg000330.
- Schott, F. A., J. P. McCreary Jr., and G. C. Johnson, 2004: Shallow overturning circulations of the tropical-subtropical oceans. *Earth's Climate: The Ocean-Atmosphere Interaction*, Wang et al., Eds., AGU, 261–304.
- Sen Gupta, A., L. C. Muir, J. N. Brown, S. J. Phipps, P. J. Durack, D. Monselesan, and S. E. Wijffels, 2012: Climate drift in the CMIP3 models. *J. Climate*, doi: 10.1175/jcli-d-11-00312.1.
- Steffen, E. L., and E. A. D'Asaro, 2002: Deep convection in the Labrador Sea as observed by Lagrangian floats. *J. Phys. Oceanogr.*, **32**(2), 475–492.
- Swingedouw, D., P. Braconnot, P. Delecluse, E. Guilyardi, and O. Marti, 2007: The impact of global freshwater forcing on the thermohaline circulation: Adjustment of North Atlantic convection sites in a CGCM. *Climate Dyn.*, **28**(2), 291–305, doi: 10.1007/s00382-006-0171-3.
- Timmermann, A., M. Latif, R. Voss, and A. Grötzner, 1998: Northern hemispheric interdecadal variability: A coupled air-sea mode. *J. Climate*, **11**(8), 1906–1931, doi: 10.1175/1520-0442-11.8.1906.
- Timmermann, A., S.-I. An, U. Krebs, H. Goosse, 2005: ENSO Suppression due to weakening of the North Atlantic thermohaline circulation. *J. Climate*, **18**, 3122–3139.
- Timmermann, A., and Coauthors, 2007: The influence of a weakening of the Atlantic meridional overturning circulation on ENSO. *J. Climate*, **20**, 4899–4919.
- Treguier, A. M., M. H. England, S. R. Rintoul, G. Madec, J. Le Sommer, and J. M. Molines, 2007: Southern Ocean overturning across streamlines in an eddy simulation of the Antarctic circumpolar current. *Ocean Science*, **3**(4), 491–507, doi: 10.5194/os-3-491-2007.
- Trenberth, K. E., J. M. Caron, and D. P. Stepaniak, 2001: The atmospheric energy budget and implications for surface fluxes and ocean heat transports. *Climate Dyn.*, **17**, 259–276.
- Van Aken, H., 2007: *Ocean Thermohaline Circulation*. Springer Verlag, New York, NY, 326 pp.
- Volodin, E., N. Diansky, R. Purini, and C. Transerici, 2009: On the mechanism of natural variability of Atlantic meridional overturning circulation in climate model INMCM3.0. Presentation at EGU General Assembly 2009, Vienna, Austria.
- Wang, B., H. Wan, Z. Ji, X. Zhang, R. Yu, Y. Yu, and H. Liu, 2004: Design of a new dynamical core for global atmospheric models based on some efficient numerical methods. *Sci. China (A)*, **47**, 4–21, doi: 10.1360/04za0001.
- Willis, J. K., 2010: Can in situ floats and satellite altimeters detect long-term changes in Atlantic Ocean overturning? *Geophys. Res. Lett.*, **37**(6), L06602, doi: 10.1029/2010gl042372.
- Wunsch, C., and D. Stammer, 1998: Satellite altimetry, the marine geoid, and the oceanic general circulation. *Annual Review of Earth and Planetary Sciences*, **26**, 219–253.
- Yashayaev, I., M. Bersch, and H. M. van Aken, 2007: Spreading of the Labrador Sea water to the Irminger and Iceland basins. *Geophys. Res. Lett.*, **34**(10), L10602, doi: 10.1029/2006gl028999.
- Zhai, X., H. L. Johnson, and D. P. Marshall, 2011: A model of Atlantic heat content and sea level change in response to thermohaline forcing. *J. Climate*, **24**(21), 5619–5632, doi: 10.1175/jcli-d-10-05007.1.
- Zhang, R., 2007: Anticorrelated multidecadal variations between surface and subsurface tropical North Atlantic. *Geophys. Res. Lett.*, **34**(12), L12713, doi: 10.1029/2007gl030225.
- Zhang, R., 2010a: Latitudinal dependence of Atlantic meridional overturning circulation (AMOC) variations. *Geophys. Res. Lett.*, **37**(16), L16703, doi: 10.1029/2010gl044474.
- Zhang, R., 2010b: Northward intensification of anthropogenically forced changes in the Atlantic meridional overturning circulation (AMOC). *Geophys. Res. Lett.*, **37**(24), L24603, doi: 10.1029/2010gl045054.